13

In Situ Observations of the Indirect Effects of Aerosols on Clouds

M.D. KING[1], SI-CHEE TSAY[1], and S. PLATNICK[2]
[1]NASA Goddard Space Flight Center, Greenbelt, Maryland 20771, U.S.A.
[2]Research and Data Systems Corporation at NASA Goddard Space Flight Center

ABSTRACT

This chapter presents an overview of our current understanding of the indirect effects of aerosol particles on cloud microphysical and radiative properties, focusing both on *in situ* and remote-sensing measurements that have led to an enhanced understanding of human impact on climate. Due to the difficulty of separating the influence of cloud condensation nuclei increases on cloud droplet concentration and hence cloud radiative properties, we concentrate our attention on stratocumulus clouds in the remote marine environment. We begin this review by defining cloud susceptibility and hence why some clouds are more likely to respond to enhanced aerosol injections than other clouds. We discuss in some detail a selected number of observations that demonstrate indirect effects and cloud susceptibility, including small-scale observations of clouds modified by aerosol emissions from ships ("ship tracks") and large-scale observations of marine stratocumulus clouds in both maritime and continental air masses, obtained during the Atlantic Stratocumulus Transition Experiment (ASTEX) conducted near the Azores in June, 1992. Finally, we will clarify the significant and complimentary roles that *in situ* microphysical and radiation instrumentation play in quantifying the indirect effects of aerosol on clouds, as well as the added value that arises from coordinating these measurements with remote-sensing observations from aircraft or satellite.

> "The conclusions which may be drawn from these experiments are—(1) that when water vapour condenses in the atmosphere, it always does so on some solid nucleus; (2) that the dust particles in the air form the nuclei on which it condenses; (3) if there was no dust in the air there would be no fogs, no clouds, no mists, and probably no rain."
>
> —*John Aitken* [1880]

Aerosol Forcing of Climate
Edited by R.J. Charlson and J. Heintzenberg. Published 1995 John Wiley & Sons Ltd.

INTRODUCTION

The concentration of cloud droplets in stratiform clouds is primarily a function of the concentration of cloud condensation nuclei (CCN) at a few tenths of 1% supersaturation, with a secondary dependence upon updraft velocity beneath cloud base (Twomey 1959; Twomey and Warner 1967). This is expected to be true in a maritime airmass in which the droplet concentration (N) is related to the supersaturation (S) according to the empirical, cloud chamber-derived formula $N = CS^k$, where k is often smaller than unity. In continental air, where k often exceeds unity, the updraft velocity below cloud base plays an increasingly important role in determining the cloud droplet concentration.

Both natural and anthropogenic aerosol particles affect cloud microstructure, cloud chemistry, and solar radiation which, in turn, lead to changes in the radiative and microphysical properties of clouds (e.g., Twomey 1980; Hudson 1983; Radke 1989). In the remote marine environment, dimethylsulfide produced by phytoplankton is believed to be the major source of CCN after oxidation to form sulfate aerosol (Bigg et al. 1984; Ayers et al. 1991; Hegg et al. 1991). Anthropogenic sources of pollution can also affect CCN concentrations and cloud droplet size distributions as shown downwind of cane fires in Australia (Warner and Twomey 1967), paper mills in the Pacific Northwest (Hobbs et al. 1970), urban cities such as Denver and St. Louis (Squires 1966; Braham 1974), the eastern seaboard of the United States (Radke and Hobbs 1976), and clouds modified by emissions from ships (Radke et al. 1989).

Increases in anthropogenic sources of CCN can increase cloud albedo by increasing the concentration and reducing the size of water droplets in water clouds. This process, usually referred to as the *indirect effect* of aerosol on climate, was first pointed out by Twomey (1974, 1977) and Twomey et al. (1984). Wigley (1989) has argued that the large increase in SO_2 emissions that has occurred in the Northern Hemisphere this century may have resulted in enhanced concentrations of sulfate particles and hence CCN, thereby increasing cloud droplet concentrations and in that way producing clouds with higher albedos in the Northern Hemisphere than in the Southern Hemisphere. This suggestion is consistent with Durkee's (1990) analysis, which was based on three years of Advanced Very High Resolution Radiometer (AVHRR) satellite observations over the Pacific Ocean, which shows that the aerosol optical thickness and cloud reflectance at 3.7 μm are approximately twice as large in the Northern Hemisphere as in the Southern Hemisphere. Rough estimates for the potential climate forcing from the indirect effect, presented by Charlson et al. (1992), suggest that particulate modification of cloud albedo can be of comparable magnitude, but opposite sign, to greenhouse-gas forcing. Platnick and Twomey (1994) have pointed out that not all clouds are equally susceptible to modification by CCN; even those in a clean marine environment can show a great variability. The susceptibility of a cloud is a function of both its albedo and droplet concentration.

The albedo increase postulated in the indirect effect is believed to be the dominant radiation influence of aerosols on clouds. However, pollution is also a source of

carbonaceous aerosol that absorbs radiation. This effect of aerosol absorption on cloud albedo, considered by Twomey (1977), Ackerman and Baker (1977), and Grassl (1982), can only be seen in bright clouds contaminated by large amounts of absorbing aerosol. For example, a net decrease in albedo of a few percent has been deduced for bright Amazonian clouds (albedo ≈ 0.7) formed during biomass burning (Kaufman and Nakajima 1993). Furthermore, Grassl found that modification of cloud microphysics by particulate pollution has little effect on cloud radiative properties in the infrared. Thus our discussion of the indirect effect must focus on microphysical changes to the shortwave forcing of clouds.

The indirect effect assumes that an increase in the number of CCN increases a developing cloud's final droplet concentration, which in turn increases cloud optical thickness and albedo. An experimental confirmation of this effect would have to show increases in each of these quantities and also, and perhaps *more* importantly, show that their increases were due solely to CCN increases and not due to dynamic and thermodynamic influences on the cloud. The difficulty is that one cannot subject a cloud to the thought experiment that implicitly accompanies the definition of the indirect effect; the existing cloud being measured cannot be asked to form all over again with more or less CCN being present, all other parameters being held constant. In other words, an experimental *control* cloud is not likely to be unambiguously present. Ship tracks, or other small-scale events, may be an exception.

In this chapter, we summarize the state of knowledge of the indirect effects of aerosol on cloud microphysical and radiative properties, focusing both on *in situ* and remote-sensing instrumentation that have had an especially profound impact on our understanding of the *in situ* effects of aerosol on clouds. We begin this review by defining cloud susceptibility and hence why some clouds respond more dramatically to enhanced aerosol injections than other clouds. We follow this discussion with an examination of significant cloud microphysics and radiation instrumentation that permit a quantitative assessment of cloud response to CCN modification. Finally, we discuss in some detail a selected number of especially striking observations that demonstrate indirect effects and cloud susceptibility, including small-scale observations of clouds modified by emissions from ships ("ship tracks") and large-scale observations of marine stratocumulus clouds in both maritime and continental air masses obtained during ASTEX conducted near the Azores in June, 1992.

CLOUD SUSCEPTIBILITY

Before looking for *in situ* measurements that confirm an indirect effect, it is necessary to determine which cloud parameters need to be measured and their relative importance to the potential modification of cloud albedo by aerosols.

The relative importance of droplet concentration and albedo to the indirect effect can easily be seen using the two-stream approximation for cloud albedo (e.g., Bohren 1987; Harshvardhan and King 1993). To simplify the approximation, we consider the

case of conservative scattering, applicable in the visible wavelength region in the absence of significant aerosol absorption, and further consider diffuse reflectance. Under conditions of constant liquid water content, the cloud optical thickness (δ_c) is proportional to droplet concentration (N) to the one-third power such that the albedo, A, becomes

$$A = \frac{(1-g)\delta_c}{a + (1-g)\delta_c} = \frac{(1-g)N^{1/3}}{c + (1-g)N^{1/3}}, \tag{13.1}$$

where a and c are constants and g is the asymmetry factor. Thus, the magnitude of the indirect effect, which is the change in cloud albedo due to a change in droplet concentration, ΔN, can be written as (Platnick and Twomey 1994):

$$\Delta A = \frac{A(1-A)\left[\left(1+\frac{\Delta N}{N}\right)^{1/3} - 1\right]}{A\left[\left(1+\frac{\Delta N}{N}\right)^{1/3} - 1\right] + 1}. \tag{13.2}$$

This approximation shows that the indirect effect depends upon A, N, and ΔN, each of which needs to be measured. At all droplet concentrations, Eq. 13.2 shows a maximum change in albedo for clouds having an existing albedo of 0.5. Furthermore, the smaller the droplet concentration (N), the larger is the increase in albedo for a given change ΔN. The two-stream approximation was adopted because of its simplicity and can, of course, be replaced by full radiative transfer calculations of albedo or reflection function for any particular solar zenith angle and observation angles. Doing so, however, does not change the physical principles outlined above.

Since ΔN is variable, it is more useful to define a figure of merit that establishes the sensitivity of cloud albedo to changes in CCN concentration as a function of the cloud's measurable parameters, A and N. Such a quantity, defined for the condition of constant liquid water content, is the *cloud susceptibility* (Twomey 1991; Platnick and Twomey 1994) given by

$$\frac{dA(\delta_c, \omega_0, g)}{dN} = \frac{\partial A}{\partial \delta_c}\frac{d\delta_c}{dN} + \frac{\partial A}{\partial \omega_0}\frac{d\omega_0}{dN} + \frac{\partial A}{\partial g}\frac{dg}{dN}, \tag{13.3}$$

where ω_0 is the droplet's single-scattering albedo. The derivative dA/dN is approximately equivalent to the change in albedo that would have occurred to an existing cloud if it had developed under identical circumstances but in a slightly "dirtier" air mass such that the final droplet concentration was increased by one droplet per unit volume, i.e., $\Delta N = 1$ (with liquid water being held constant). The approximate linearity

between CCN and N, or some other determined relationship, can be invoked to calculate dA/dCCN. Note that the change in forcing is proportional to susceptibility, i.e., $dF/dN = F_0\, dA/dN$, where F is the reflected flux and F_0 the incident solar flux at cloud top.

As was done above, consider susceptibility in the visible, where about one-half of the solar flux occurs. With $\omega_0 = 1$ and g being approximately constant with radius, susceptibility reduces to

$$\frac{dA(\delta_c, \omega_0, g)}{dN} \cong \frac{\partial A}{\partial \delta_c}\frac{\delta_c}{3N} \cong \frac{4\pi\rho_w}{9W}\delta_c\left(\frac{\partial A}{\partial \delta_c}\right) r^3 , \tag{13.4}$$

where r is droplet radius, W the cloud liquid water content, and ρ_w the density of liquid water. Strictly speaking, in Eq. 13.4, r is approximately the volume-weighted moment of the droplet size distribution (Platnick and Twomey 1994), defined as

$$r_v = (\overline{r^3})^{1/3} . \tag{13.5}$$

Both remote-sensing techniques and *in situ* instrumentation report values of the effective radius, defined as

$$r_e = (\overline{r^3})/(\overline{r^2}) . \tag{13.6}$$

The work of Grassl (1982) and Martin et al. (1994) suggests that the difference between r_e and r_v is minor compared to other measurement uncertainties. For example, Martin et al., in analyzing marine stratocumulus near California and the United Kingdom, developed the regression $r_v \cong 0.93 r_e$ (or $r_v^3 \cong 0.8 r_e^3$) for all clouds that they sampled. As with Eq. 13.2, susceptibility shows ΔA depending upon the three parameters: A, N, and dN. Furthermore, the term $\delta_c\, \partial A/\partial \delta_c$ that appears in Eq. 13.4 yields a maximum susceptibility for clouds having an albedo of 0.5 at all droplet concentrations or droplet radii. Since albedo in the visible is a weak function of effective radius, the calculation for this term has generally been made by a full radiative transfer calculation. However, for illustrative purposes, we show in Figure 13.1 surface plots of susceptibility based on the two-stream approximation.

Note that susceptibility is inversely proportional to droplet concentration or, alternatively, varies proportionally to the radius cubed and inversely with liquid water content. The second form in Eq. 13.4 is especially useful with remote-sensing measurements since droplet size, but not concentration, can be inferred from reflection measurements (e.g., Twomey and Cocks 1989; Rawlins and Foot 1990; Nakajima et al. 1991). With this form, however, an assumption, or other measurement, must be used for liquid water content. From *in situ* measurements, it is straightforward to determine N or, alternatively, r and W. However, reflection measurements obviously provide an easier and more direct means of estimating the cloud optical thickness.

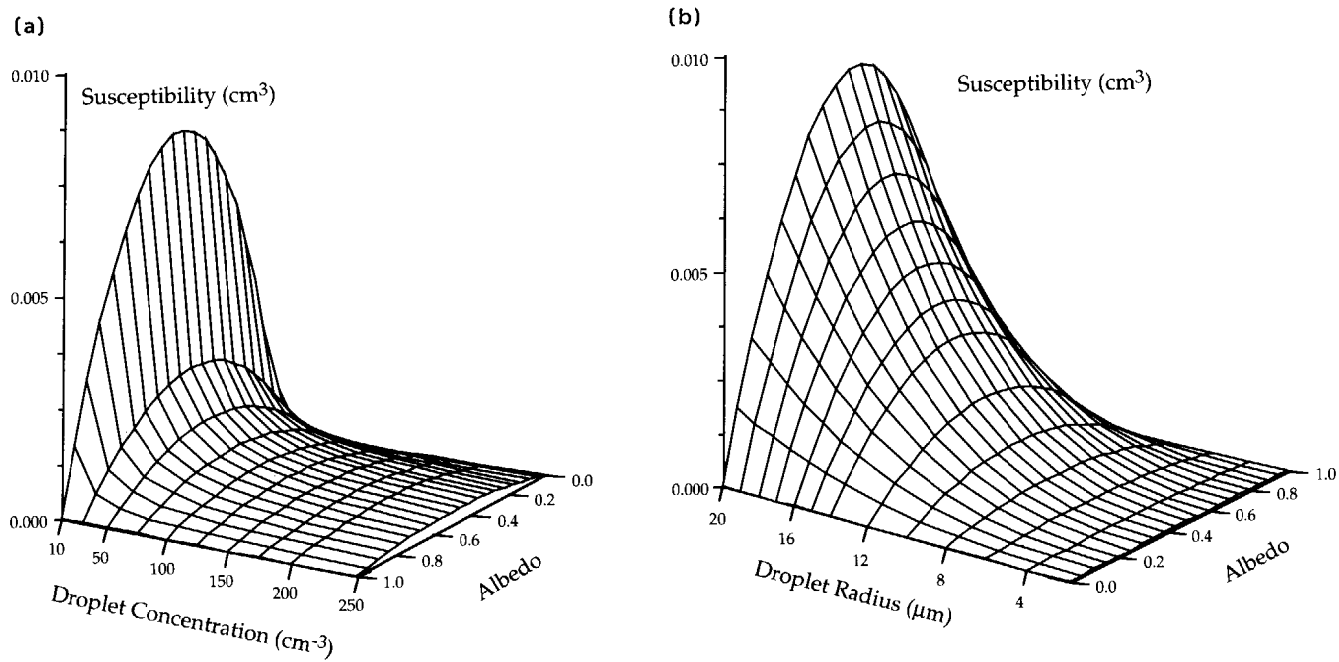

Figure 13.1 Cloud susceptibility as a function of cloud albedo and (a) droplet concentration and (b) effective radius with liquid water content equal to 0.3 g m^{-3}. These calculations are based on a two-stream approximation (see text for details).

Susceptibilities retrieved with the 3.7 μm channel on the AVHRR in selected California stratus vary over an order of magnitude (Platnick and Twomey 1994), from about 0.5 $\times 10^{-3}$ to 10×10^{-3} cm^3. Note that a susceptibility of 10×10^{-3} cm^3 means that if the cloud's droplet concentration were to increase by just 1 cm^{-3}, the albedo would increase by 0.01, resulting in a 1% increase in radiative forcing.

Susceptibility is useful in two ways. Referring back to the previous section, the typical absence of well-defined control clouds makes it difficult to verify that the indirect effect has taken place. For cases where albedo and droplet concentration have been determined, susceptibility can provide a useful inference; susceptibility will decrease as a cloud experiences the indirect effect giving a relative indication of the magnitude of perturbation. Second, susceptibility estimates the magnitude of *potential* albedo modification to existing clouds, and therefore changes in cloud forcing.

CURRENT INSTRUMENTATION

While an *in situ* measurement of droplet concentration is conceptually straightforward, an *in situ* determination of albedo from local measurements requires a determination of optical thickness, which in turn implies a vertical integration involving droplet concentration and droplet radius. It is more common for albedo to be inferred from airborne or satellite reflectance measurements. However, such a radiation measurement is not usually considered *in situ* even though, in this case, the radiance measurement *is* the most direct measurement of albedo. For present purposes, both microphysics and radiation measurements will be used to search for the indirect effect.

To deduce the indirect effects of aerosols on clouds on a small-scale, assuming constant background meteorology, *in situ* measurements of the cloud drop size distribution $n(\delta, r_e)$ and angular distribution of the reflection function $R(\delta_c, \mu)$ at a vertical coordinate δ are essential. On the other hand, to infer large-scale indirect effects on clouds, the remotely sensed cloud albedo A and retrieved cloud optical thickness δ_c and effective particle radius r_e are vital. Instruments used to measure the aforementioned parameters that are directly related to this review are briefly discussed below.

Cloud Microphysics Instrumentation

The primary cloud microphysics probes commonly used to measure the cloud droplet size distribution are the Forward Scattering Spectrometer Probe (FSSP–100) and Optical Array Cloud and Precipitation Probes (OAP–200X and OAP–200Y), manufactured by Particle Measuring Systems, Inc. (Knollenberg 1981). These provide essentially continuous measurements of cloud droplet size distributions over the radius range 1.4–2250 μm at sampling rates up to 1000 Hz. When the FSSP measures cloud droplets under high concentrations, coincidence or dead-time corrections are required, as described by Baumgardner et al. (1985) and Brenguier (1989). The cloud liquid

water content and effective particle radius can readily be derived by direct integration over the size distribution.

Recently, a new microphysics sensor, the Particulate Volume Monitor (PVM–100A), developed by Gerber Scientific Inc. (Gerber et al. 1994), was successively developed and operated during the ASTEX campaign. This probe simultaneously measures the cloud liquid water content and integrated particle surface area (PSA). The ratio of these two parameters determines the effective particle radius. The PVM–100A samples many particles simultaneously at a maximum rate of 5 kHz and with a sampling volume of 1.25 cm^3. This sampling volume is about 50,000 times larger than that of the FSSP–100, which measures individual particles. Also, unlike the FSSP–100, the PVM–100A is independent of air speed, permitting it to measure liquid water content more accurately.

During ASTEX, the PVM–100A was flown on the University of Washington's C–131A research aircraft on sixteen flights, and was co-located near the Johnson-Williams and King hot-wire probes and the FSSP–100 probe. Figure 13.2 shows an intercomparison between these four probes. It is clear from this figure that the two hot-wire probes (10 Hz data) are unable to resolve fine-scale features in broken clouds because of the slow response time of the hot wire probes. Figures 13.2a and 13.2b clearly show that there is a large difference in the effective particle radius derived from the FSSP–100 (1 Hz data) and the PVM–100A (10 Hz data). These figures also show that the FSSP–100 underestimates liquid water content when either the liquid water content or particle sizes are large. Figures 13.2c and 13.2d show a time series obtained near cloud top (where the drops are the largest in stratocumulus) and cloud base (where the drops are small), respectively. The differences between the FSSP–100 and the PVM–100A measurements reflect the time-response error of the uncorrected FSSP–100, which causes large underestimates of particle sizes. Since the PVM–100A provides only bulk microphysical parameters, drop size distributions (which are necessary quantities for radiation applications) must still be obtained from FSSP–100 measurements. By flying both probes together on the C–131A, and adopting the correction method described by Gerber et al. (1994), the accuracy of the drop size spectra derived from the FSSP–100 can be substantially improved.

Cloud Radiation Instrumentation

Three radiometric sensors that measure the scattered radiation field will briefly be described here. These are the Cloud Absorption Radiometer (CAR), the MODIS Airborne Simulator (MAS) and the Advanced Very High Resolution Radiometer (AVHRR).

The CAR is a multiwavelength scanning radiometer (King et al. 1986) that is mounted on the University of Washington's Convair C–131A research aircraft. The CAR measures the angular distribution of scattered radiation at thirteen discrete wavelengths between 0.31 μm and 2.3 μm or 0.47 μm to 2.3 μm, depending on configuration, and scans in a vertical plane on the right hand side of the aircraft from

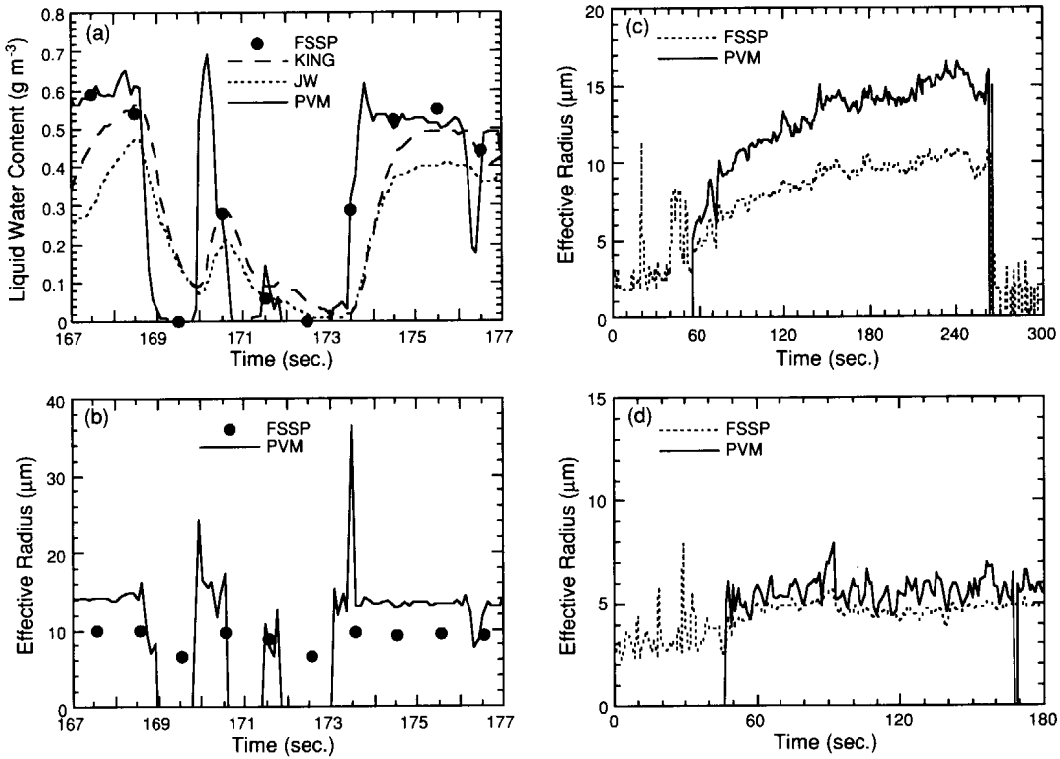

Figure 13.2 Intercomparison between the PVM–100A, FSSP–100, Johnson-Williams hot wire, and King hot wire probes for (a) liquid water content and (b) effective radius as a function of time over a broken cloud field, and (c) measurements near cloud top for 5 min of data and (d) near cloud base for 3 min of data.

5° before zenith to 5° past nadir (190° aperture). This permits observations of both the zenith and nadir intensities to be obtained with as much as a 5° aircraft roll, an angle that is measured by a gyroscope aboard the Convair.

The instantaneous field of view of the CAR is 1° (17.5 mrad), a spatial resolution of 35 meters at nadir from a nominal C–131A altitude of 2 km. The filter wheel contains optical channels 8 through 13 and can be locked at a particular channel or rotated to measure a new wavelength interval after a preset number of scans. With this configuration, the first seven channels are continuously and simultaneously sampled, while the eighth registered channel is selected from among the six channels on the filter wheel. All of the CAR channels were carefully selected to minimize gaseous absorption, unless specifically required (such as the UV–B ozone channel). Since the scan rate of the CAR is 1.67 Hz (100 rpm), the full angular distribution of scattered radiation from zenith to nadir is sampled every 48 m at a nominal aircraft speed of 80 m sec^{-1}.

The MAS is a scanning spectrometer, built by Dædalus Enterprises for Goddard Space Flight Center and Ames Research Center, and was designed for the purpose of measuring the reflected solar and emitted thermal radiation in 50 narrow bandwidth channels between 0.55 μm and 14.3 μm. Nineteen of the channels on the MAS have corresponding spectral characteristics on the MODIS (cf. Salomonson et al. 1989; King et al. 1992), a satellite sensor being developed for the Earth Observing System (EOS) to be launched in the late 1990s.

The MAS has a 2.5 mrad instantaneous field of view and scans perpendicular to the aircraft flight track with a scan angle of ± 43° about nadir, thereby providing images with a spatial resolution of 50 m at nadir and a 37 km swath width from a nominal ER–2 aircraft altitude of 20 km. The roll correction of the MAS can be as large as ±15°. There are four detector arrays in the MAS optical system as follows: (a) 9 channels between 0.50–0.99 μm with a bandwidth of ~0.04 μm, (b) 16 channels in the 1.57–2.42 μm region with a bandwidth of ~0.05 μm, (c) 16 channels in the 2.85–5.40 μm region with a bandwidth of ~0.15 μm, and (d) 9 channels in the 8.15–14.7 μm region with a bandwidth of 0.4–0.5 μm. The scan rate of the MAS is 6.25 Hz (375 rpm).

The AVHRR is a cross-track scanning radiometer flown aboard the NOAA near-polar, sun-synchronous satellite. The current generation of the AVHRR features five spectral channels: 0.58–0.68 μm, 0.725–1.10 μm, 3.55–3.93 μm, 10.30–11.30 μm, and 11.50–12.50 μm. The instantaneous field of view of each channel is approximately 1.4 mrad, leading to a spatial resolution of 1.1 km at satellite subpoint from a nominal altitude of 833 km. With a scan angle of ± 55.4°, the AVHRR image covers a swath width of more than 2,000 km on Earth. The scan rate of the AVHRR is 6 Hz (360 rpm).

EXAMPLES OF INDIRECT EFFECTS

Small-scale Observations: Ship Tracks

A striking example of the effects of anthropogenic CCN on cloud radiative properties can be found in satellite observations of marine stratocumulus clouds modified by

emissions from ships. These so-called "ship tracks" were first observed in satellite imagery under conditions in which exhaust particles emitted by ships were responsible for producing a visible cloud in otherwise cloud-free conditions (Conover 1966). Coakley et al. (1987) and Albrecht (1989) observed the frequent and long-lived occurrence of ship track signatures in preexisting stratus and stratocumulus clouds, as evident by the enhanced reflectance of these clouds, especially at 3.7 μm. During the marine stratocumulus intensive field observation (IFO) component of the First ISCCP Regional Experiment (FIRE), conducted off the coast of southern California during July, 1987 (Albrecht et al. 1988), the first *in situ* microphysics and solar radiation measurements of clouds modified by pollution from ships were obtained. Selected radiative and microphysical properties of these clouds, together with AVHRR satellite images, have been described by Radke et al. (1989) and King et al. (1993).

Plate 13.1 shows an example of marine stratocumulus modified by emissions from ships. These observations, obtained from the NOAA–9 AVHRR as it passed over the Pacific Ocean off the west coast of California on June 27, 1987, at 2245 UTC, clearly show the enhanced reflectance of these clouds, especially at 3.7 μm. The inset, obtained from reflected solar radiation measurements at a visible wavelength of 0.63 μm, shows a less pronounced enhancement of cloud reflectance because the clouds, for the most part, are already optically thick and hence not significantly brightened by injection of additional CCN. Marine stratocumulus in the pristine maritime environment west of the U.S. mainland seem especially susceptible to modification by aerosol emissions from ships, but do not always occur. Ship track development no doubt depends upon environmental conditions such as droplet concentration and optical thickness of the preexisting clouds but may also be affected by wind speed as well as updraft velocity and turbulence structure in the marine boundary layer.

The clearest confirmation of cloud microphysics and radiation changes resulting from aerosol emissions from ships occurred on July 10, 1987, when the University of Washington C–131A aircraft flew through a pair of roughly parallel ship tracks off the coast of southern California during FIRE (Radke et al. 1989). On this day, the C–131A was flying within a marine stratocumulus cloud layer about 400 m thick enroute to a coordinated mission with the NASA ER–2 aircraft when it encountered two anomalous regions of cloud, each approximately 10–15 km in width, that exhibited substantial differences in cloud radiative and microphysical properties from those of the surrounding cloud. A GOES–6 visible image of this cloud system, together with the flight track of the C–131A between 8:50 and 9:15 PDT, can be found in King et al. (1993). These anomalous regions of cloud were located ~300 km WSW of the airfield on Coronado Island, San Diego.

Both the cloud microphysics (Johnson-Williams hot wire and PMS probes) and cloud radiation (CAR) measurements aboard the C–131A indicate that cloud radiative and microphysical properties changed dramatically in both ship tracks (Figure 13.3). Figures 13.3a and 13.3b show the droplet concentration and effective radius as a function of distance (or time) for measurements obtained inside clouds between 0850 and 0915 PDT. These results, obtained from the size distribution measurements

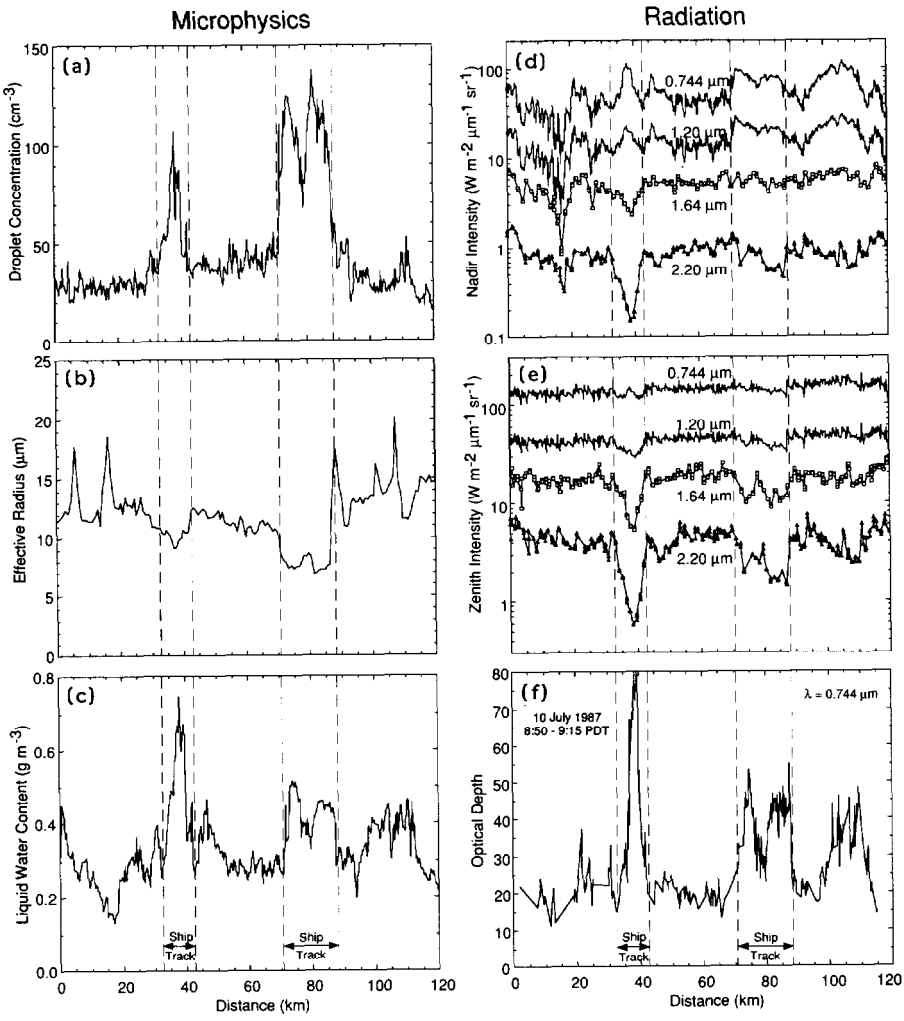

Figure 13.3 Aircraft transects of the two ship tracks on July 10, 1987, showing changes in (a) the total concentration of droplets, (b) the effective radius, (c) the cloud liquid water content, (d) the nadir (upwelling) intensities at selected wavelengths between 0.744 μm and 2.20 μm, (e) the zenith (downwelling) intensities, and (f) the total optical thickness of the cloud at 0.744 μm.

obtained from the FSSP–100 and OAP–200X probes, clearly show the strong increase in droplet concentration and decrease in effective radius in both regions of cloud affected by ships, as predicted by Coakley et al. (1987). Figure 13.3c shows a corresponding time series of cloud liquid water content measured with the Johnson-Williams hot wire probe, and demonstrates that the liquid water content was

substantially enhanced in both ship tracks, as first reported and explained by Radke et al. (1989). A clear illustration of the suppression of drizzle droplets that results from this "seeding" by CCN from the ships beneath the cloud, can be found in King et al. (1993), a figure that is reproduced in Kaufman (this volume).

Figures 13.3d and 13.3e illustrate the nadir (upwelling) and zenith (downwelling) intensities as a function of distance (time) for measurements obtained inside cloud for the same 120 km section of cloud described above. These data, corresponding to observations obtained with the CAR at four wavelengths between 0.744 μm and 2.20 μm, clearly show that the internal scattered radiation field was substantially modified by the ships as well. At $\lambda = 0.744$ μm, a weakly absorbing wavelength, the upwelling intensity increased from approximately 40 –110 W m^{-2} μm^{-1} sr^{-1} in the first ship track, with a somewhat less dramatic, though more uniform, increase in the second ship track. At $\lambda = 2.20$ μm, on the other hand, both the zenith and nadir intensities decreased substantially within the ship track features, due in part to the fact that this wavelength has substantial absorption by liquid water.

The radiative characteristics presented in Figures 13.3d and 13.3e can be understood as follows. As the cloud droplet concentration and liquid water content increase and the effective radius decreases within the ship track features, the total optical thickness of the cloud necessarily increases (as confirmed by enhanced reflection of these clouds as observed by satellite). The additional scattering leads in turn to increased attenuation of solar radiation at water absorbing wavelengths, such as 1.64 and 2.20 μm. Figure 13.3f illustrates a time series of the total optical thickness of the cloud layer at 0.744 μm inferred from a quantitative analysis of the CAR measurements presented in Figures 13.3d and 13.3e, which required a careful analysis of the similarity parameter (and hence single-scattering albedo) of the clouds as a function of time, and further took into account the fact that the solar zenith angle changed from 56.7° at the beginning of the time series to 52.6° at the end. Finally, these results suggest that the single-scattering albedo increased within the ship tracks, relative to the uncontaminated cloud, suggesting that the reduced droplet size within the ship tracks dominated any soot particle emissions from the ships (see King et al. 1993 for details).

Figure 13.4 shows a summary of both the microphysical and radiative properties of uncontaminated cloud and cloud modified by emissions from ships, and is based on our analysis of the data presented in Figure 13.3 at 63 km and 38 km, respectively. These results, taken together, are clear evidence of the indirect effect of aerosols on cloud microphysics, and hence radiative, properties.

Large-scale Observations: Marine Stratocumulus from ASTEX

For marine clouds, the initial, and maximum, cloud droplet concentration is proportional to the CCN concentration present during cloud development (Twomey 1959). Measurements by Twomey and Warner (1967) in small to moderate nonprecipitating cumuli off the coast of Queensland, Australia verified an approximately linear fit

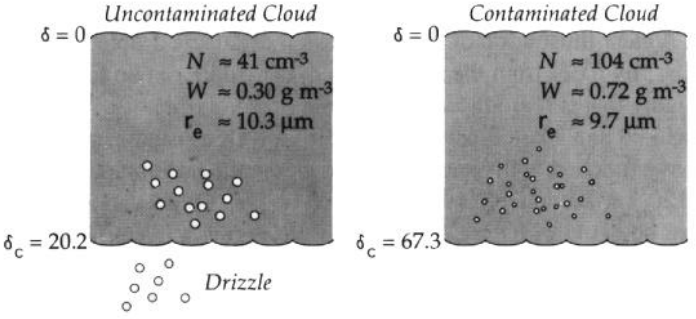

Figure 13.4 Summary of the radiation and microphysical characteristics of uncontaminated cloud and cloud contaminated by emissions from ships, based on characteristics of the cloud observed on July 10, 1987, at 63 km and 38 km, respectively.

between droplet and CCN concentrations. Similar results have been obtained in recent studies by Hudson and Rogers (1986) and Hegg et al. (1991). Therefore, cloud droplet concentration alone is likely to provide a good indication of the CCN concentrations that were made available to a cloud, an essential quantity in searching for the indirect effect. However, at the risk of being redundant, the number concentration alone cannot provide an estimate of albedo modification and therefore cannot definitively determine an occurrence of the indirect effect; a cloud's albedo must also be known along with a control cloud reference. In short, measured cloud droplet concentrations provide necessary but not sufficient data for the determination of an indirect effect. With this in mind, we look for this part of the indirect effect in measured cloud microphysical quantities collected by the Convair C–131A on June 12 and 17, 1992, during ASTEX. In the same geographical location, clouds on these two days showed significant differences in their microphysical properties, indicating different air mass origins. Retrievals of optical thickness in a few selected areas were performed using AVHRR data on June 12 and MAS data on June 17, results that will be used to calculate cloud susceptibility.

General Meteorology

On June 12, 1992, the C–131A flew to a region southeast (~35.3°N, 26°W) of Santa Maria island (36.9°N, 25.2°W), back to Santa Maria, and then to the east (~36.7°N, 23.8°W) between 0933 and 1446 UTC. During this time, the area around Santa Maria was covered in a relatively uniform stratus, but broken clouds dominated the area just south of the island. A surface high was located near 33°N, 30°W and low-level winds at Santa Maria were out of the north–northeast. Surface back-trajectories indicated that the air over the last few days had come out of the west–northwest (Bluth and Albrecht 1993). NASA's ER–2 aircraft was equipped with a monostatic cloud lidar system (CLS; Spinhirne et al. 1989) that placed the stratocumulus cloud tops at about 1 km,

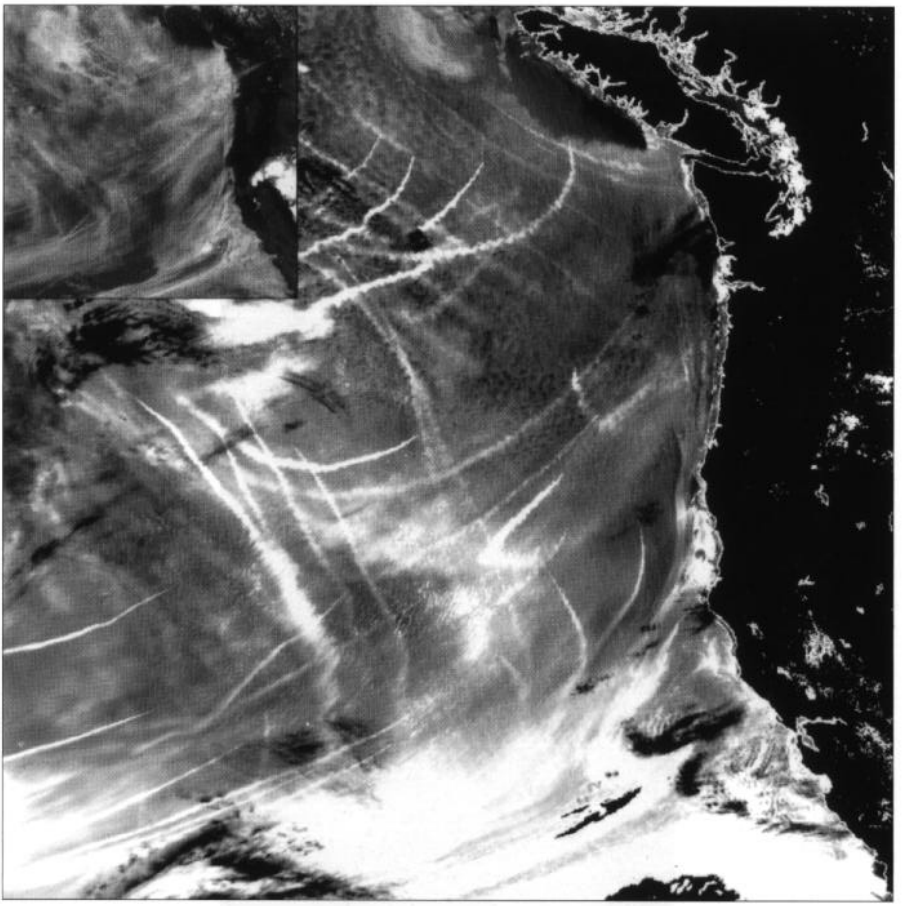

Plate 13.1 Satellite images showing an extensive stratocumulus cloud system off the West Coast of the U.S. The large image was constructed from NOAA–9 AVHRR data on June 27, 1987, at a shortwave infrared (3.7 μm) wavelength, whereas the inset was constructed from reflected solar radiation measurements at a visible (0.63 μm) wavelength. The streaks revealed at 3.7 μm are due to a reduced droplet size in clouds contaminated by the exhausts of ships.

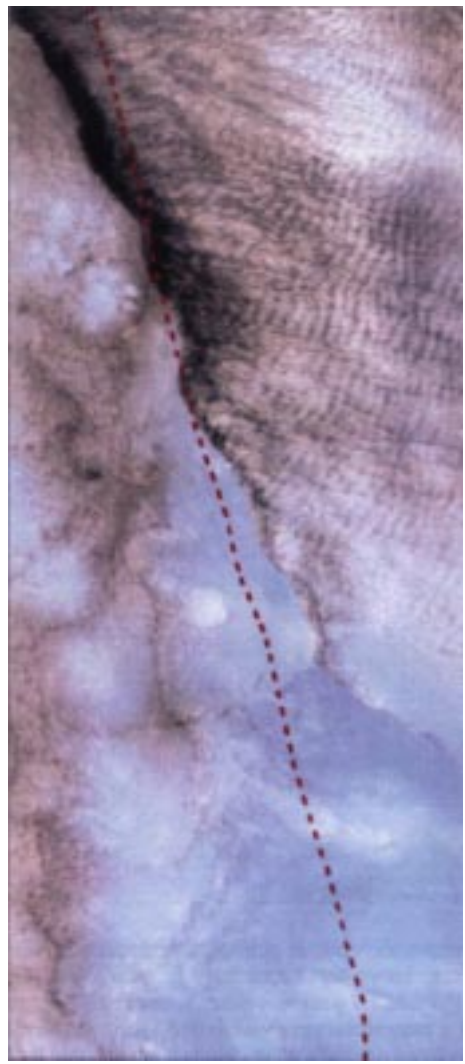

Plate 13.2 A red (2.14 μm), green (1.62 μm), and blue (0.66 μm) composite image of marine stratocumulus clouds in the eastern Atlantic, derived from 2320 scan lines of MODIS Airborne Simulator (MAS) data on June 17, 1992, between 1221:21 and 1227:33 UTC. The dashed line superimposed on this image represents the location of the University of Washington C-131A *in situ* observations presented in Figure 13.6.

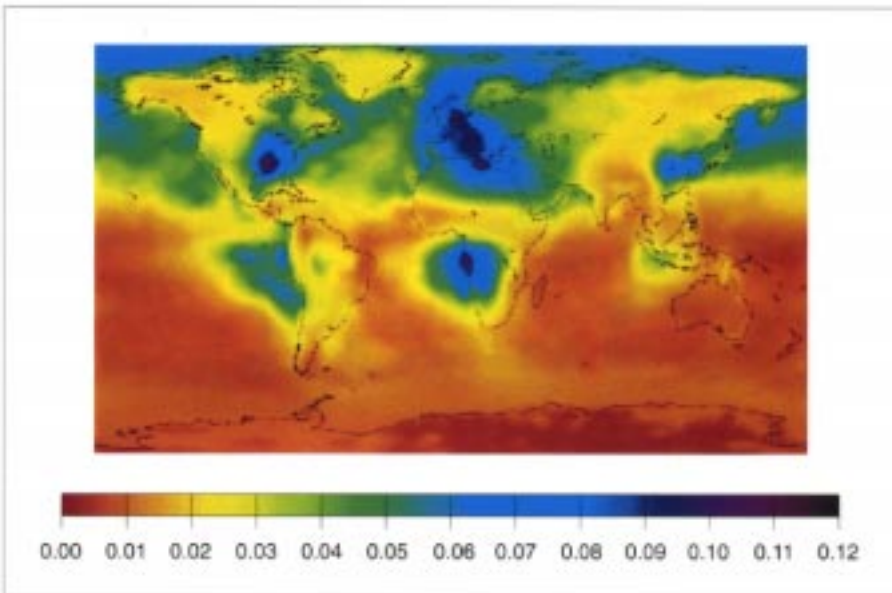

Plate 15.1 Global distribution of the sulfate aerosol visible (0.5-0.7 μm) optical depth (July), based on the Langner and Rodhe (1991) sulfate data.

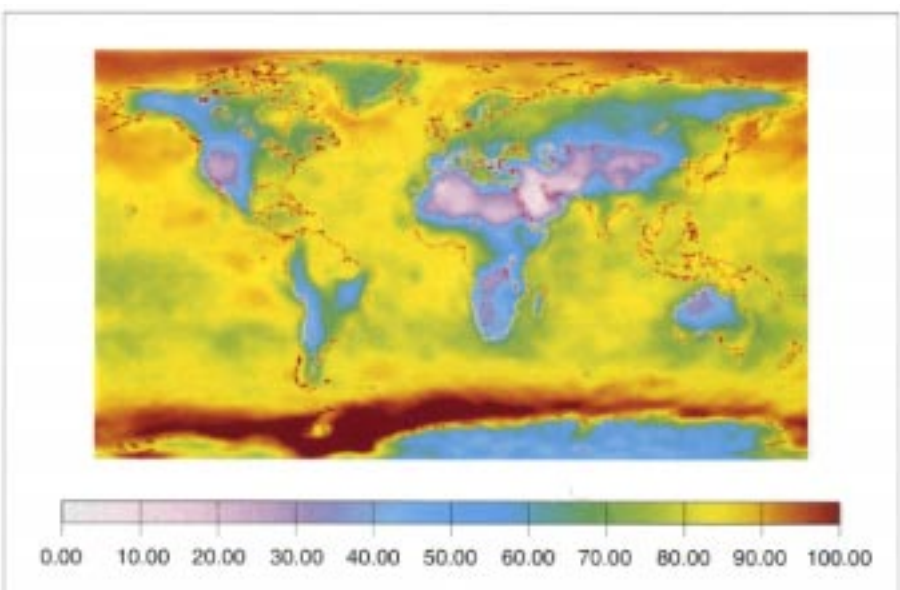

Plate 15.2 The spatial distribution of boundary layer relative humidity (%) for July obtained from the ECMWF analyses.

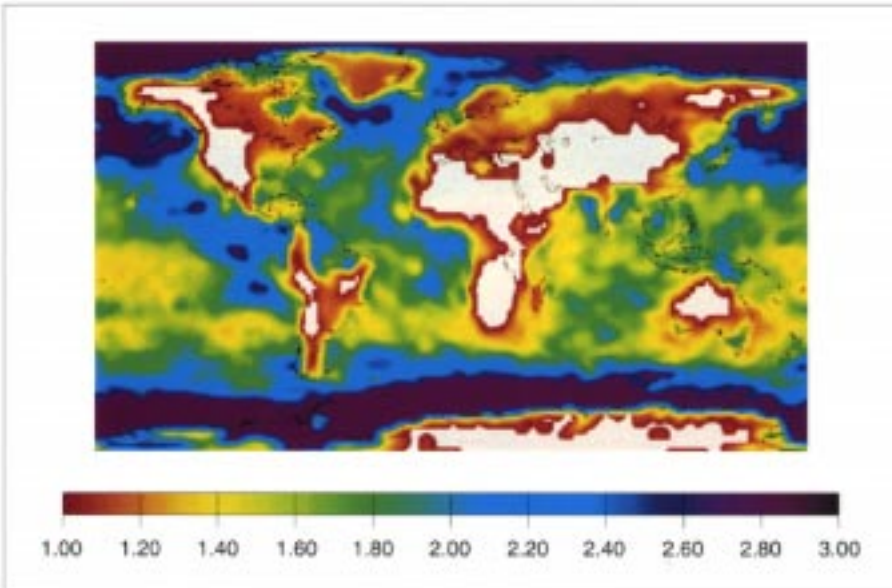

Plate 15.3 Spatial distribution of the scattering factor illustrated in Figure 15.3, maximum value is 2.8.

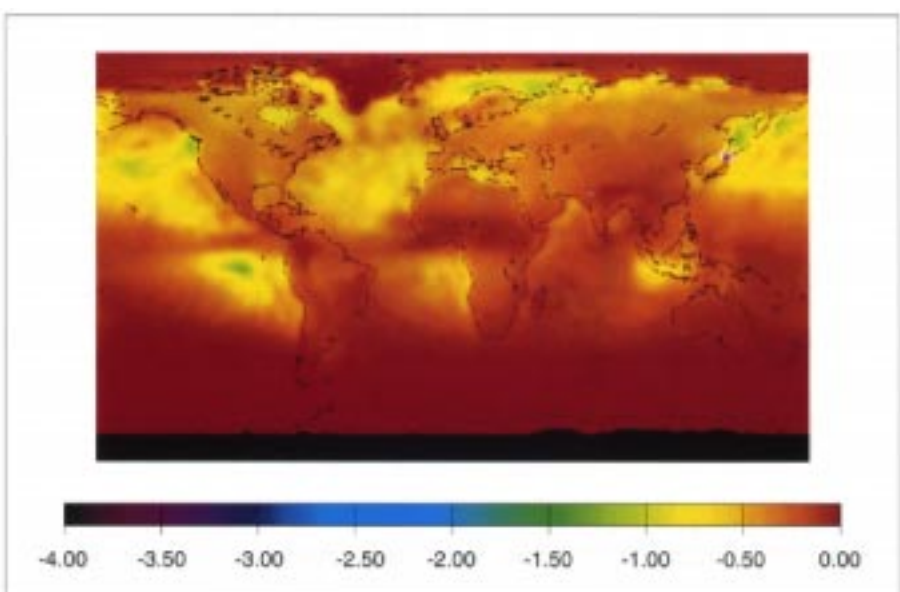

Plate 15.4 The July monthly meangeographic distribution in direct forcing (W m^{-2}) of sulfate aerosols due to natural sources from Langner and Rodhe (1991).

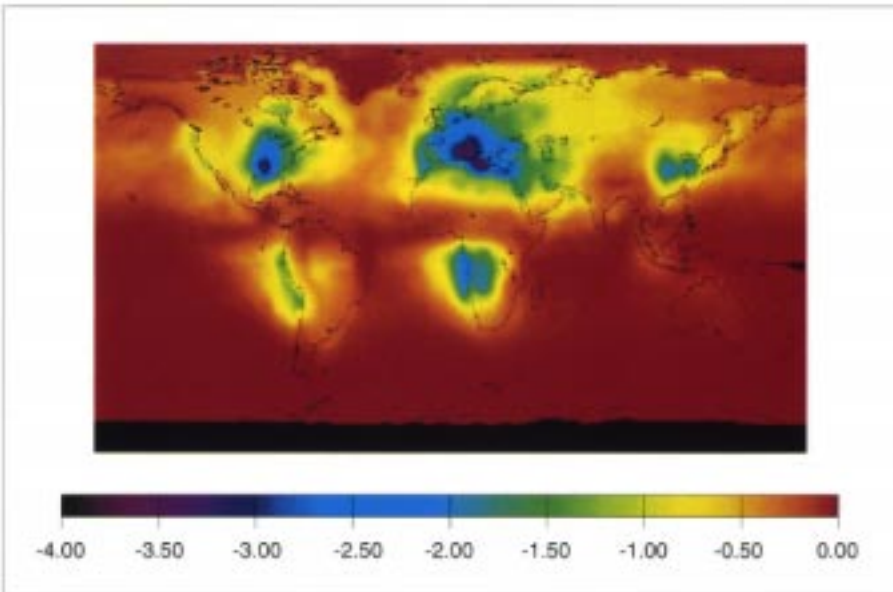

Plate 15.5 The July monthly mean geographic distribution in direct forcing (W m^{-2}) of sulfate aerosols due to anthropogenic sources from Langner and Rodhe (1991).

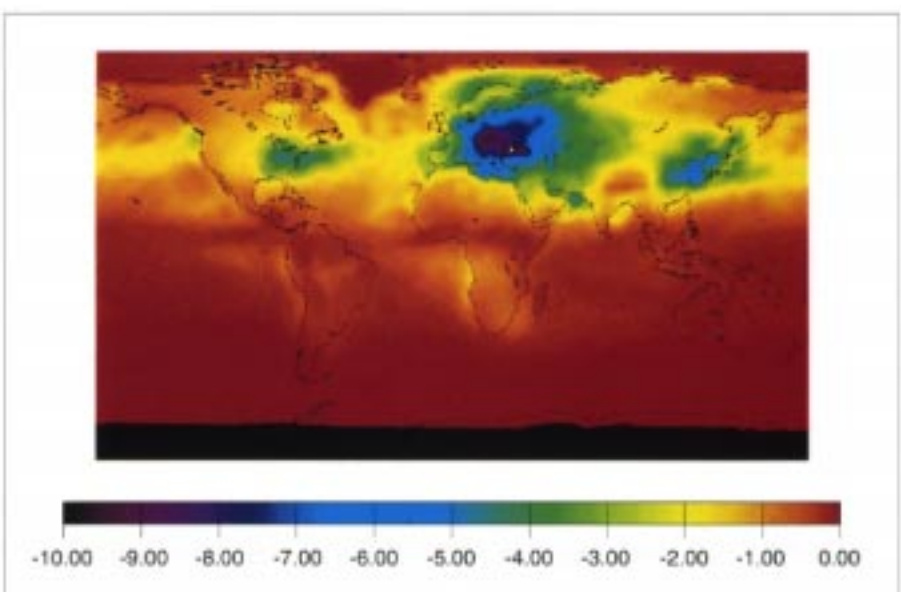

Plate 15.6 The July mean geographic distribution in anthropogenic direct forcing (W m^{-2}) using the same sulfate aerosol optical properties as in Plates 15.4 and 15.5, but the sulfate aerosol abundance from Pham et al. (submitted).

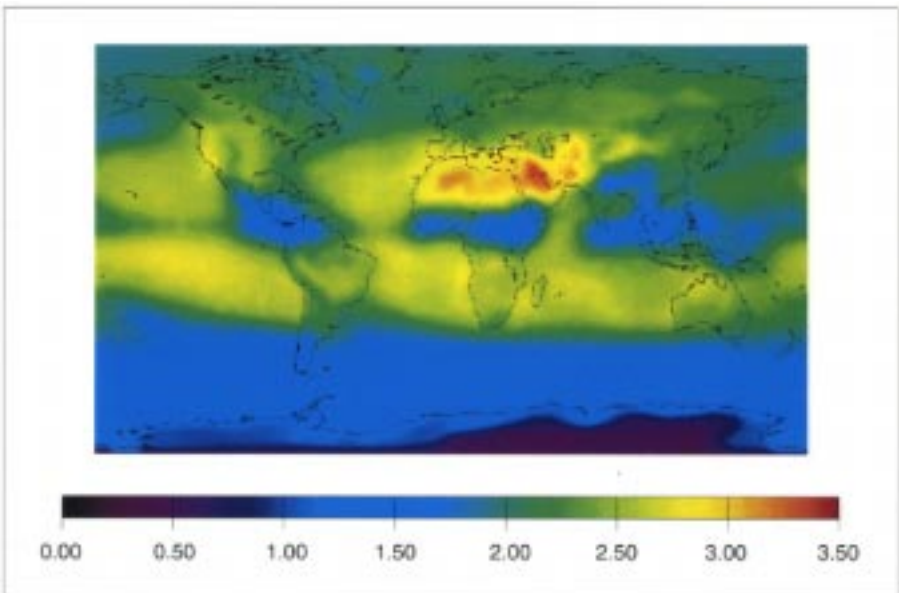

Plate 15.7 The geographicdistribution ofgreenhouse forcing (Wm^{-2}) for July due to increases in CO_2, CH_4, N_2O, CFC11, and CFC12 from the preindustrial era to the present.

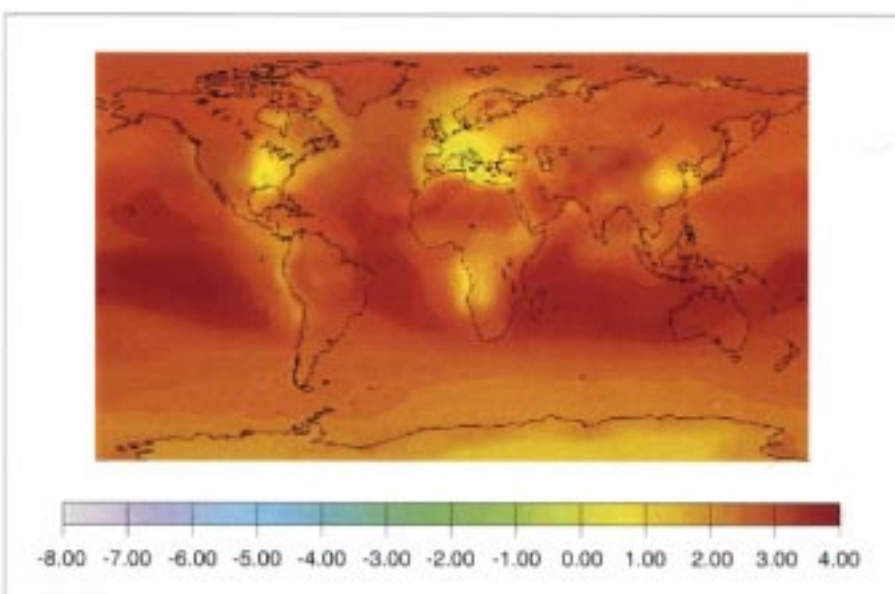

Plate 15.8 The July net forcing (Wm^{-2}) due to the greenhouse gases plus the sulfate aerosol forcing from Langner and Rodhe's (1991) sulfate data.

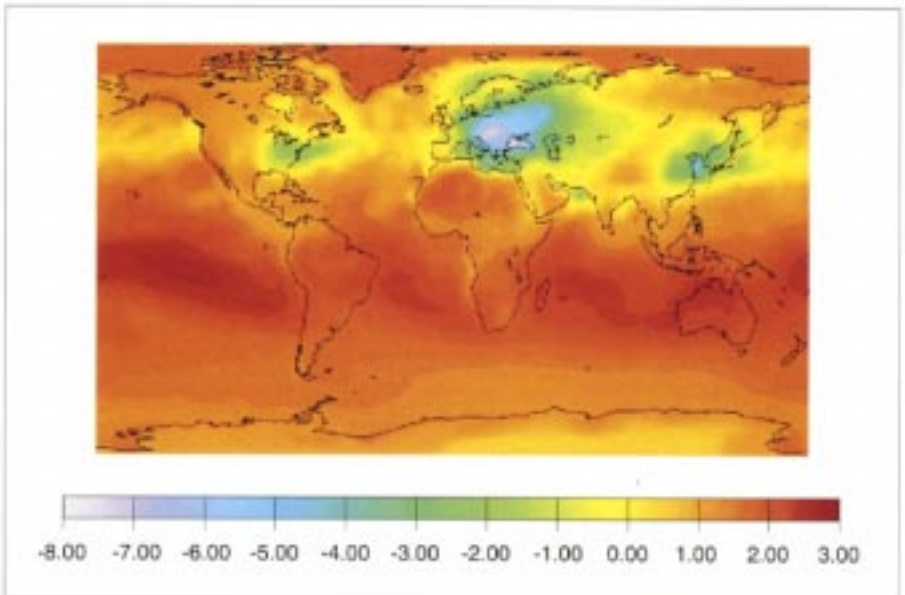

Plate 15.9 The July net forcing (Wm^{-2}) due to the greenhouse gases plus the sulfate aerosol forcing from Pham et al. (submitted) sulfate data.

while the 1200 UTC soundings at Santa Maria showed the cloud base and cloud top heights to be at 1 km and 1.3 km, respectively (Syrett 1993).

Five days later, on June 17, 1992, a high pressure system over the British Isles and a low over the southern coast of Spain produced an east to northeast lower level flow in the region of Santa Maria eastward. The C–131A flew east to about 35.8°N, 23.0°W and then back to the island of Terceira (38.8°N, 27.2°W) from 0910 to 1400 UTC. Broken stratocumulus was observed over this entire region. The CLS detected cirrus during much of its flight over the same region with stratocumulus heights measured at about 1 km. Dense haze, both above and below cloud, was noted in this area by both the C–131A and the NCAR Electra. Surface back-trajectories showed that the air mass originated to the northeast off the coast of Spain and France (Bluth and Albrecht 1993). A Santa Maria sounding at 1200 UTC showed cloud base and cloud top heights at 0.75 km and 1.1 km, respectively (Syrett 1993).

Cloud Microstructure

Frequency distributions of cloud droplet concentration, obtained from the FSSP–100 and averaged over 1 sec intervals for both days, are shown in Figure 13.5. The entire day's flight is included in the statistics, but with the requirement that simultaneously measured cloud liquid water content be greater than 0.05 g m^{-3}, thereby assuring that the measurements were obtained inside the clouds. However, the shape of the frequency distributions is not sensitive to this threshold value. The distinct differences in droplet concentration between these two days suggest that the clouds sampled by the C–131A in this region likely developed in a clean maritime air mass for June 12 and a relatively dirty, or continental, air mass for June 17.

Statistics of other C–131A microphysical measurements for these two days are summarized in Table 13.1. Condensation nuclei (CN) measurements for both above-cloud and below-cloud air show that concentrations on June 17 are a factor of three to five greater than those on June 12. Furthermore, on June 17 the mean droplet concentration is larger (395 cm^{-3}) than on June 12 (144 cm^{-3}), with a correspondingly smaller mean effective radius (9.9 μm vs. 12.7 μm) and a larger mean liquid water content (0.40 g m^{-3} vs. 0.34 g m^{-3}). All microphysical parameters obtained on June 17 show a larger spread (standard deviation) than those acquired on June 12. All indications are that, as a group, the stratocumulus on June 12 was formed in much cleaner air than the clouds on June 17. It is significant that a large difference in maritime cloud microphysics is observed in the same geographical area (~1000 km off the European continent) only a few days apart. Obviously, not all maritime-located clouds have equivalent microphysics and cannot be modeled as such.

Susceptibility

We have estimated the cloud susceptibility in selected regions of cloud on both days based in part on cloud optical thickness and effective radius retrievals using AVHRR

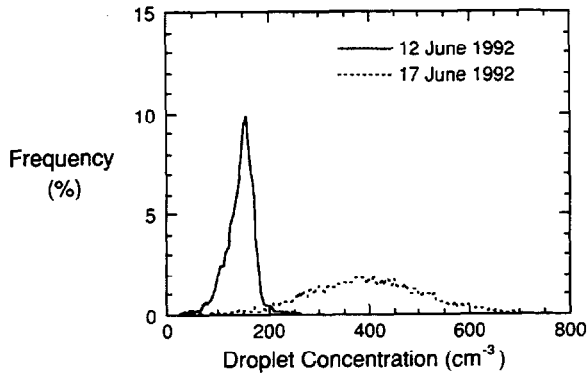

Figure 13.5 Probability distribution of cloud droplet concentration on June 12, 1992, (maritime airmass) and June 17, 1992, (continentally influenced airmass) for marine stratocumulus clouds near the Azores, Portugal, obtained from the University of Washington C–131A during ASTEX.

data on June 12, 1992, and MAS data on June 17, 1992. Retrievals of effective radius and optical thickness on June 12 were obtained using the 0.63 μm and 3.74 μm channels of the NOAA–12 AVHRR (Platnick and Valero 1995). The NOAA–12 overpass was coincident with the ER–2 and the C–131A in a region of extensive cloud southeast of Santa Maria. A visible radiometer on the ER–2 was used to calibrate channel 1 of the AVHRR (0.63 μm). The optical thickness retrieved in this region was $\delta_c = 15$, with an effective radius $r_e = 10$–12 μm. In the same area, the C–131A recorded ~10 minutes of data which resulted in a mean droplet concentration of ~103 cm^{-3} and PVM–100 measurements of effective radius $r_e = 13$–15 μm and a mean liquid water content $W = 0.40$ g m^{-3}. Based on radiative transfer calculations for $\delta_c = 15$ and $r_e = 14$ μm, we obtained $\delta_c \, \partial A/\partial \delta_c = 0.215$. Substituting this value and $N = 100$ cm^{-3} back into Eq. 13.4, we estimate the cloud susceptibility in this location to be $\sim 0.72 \times 10^{-3}$ cm^3.

To retrieve cloud optical thickness and effective radius for June 17 is more complicated than for June 12 for the following reasons: (a) a more complex cloud morphology, as observed by the MAS, (b) contamination of dense haze aloft, and (c) cirrus clouds over a large portion of the stratocumulus. Nonetheless, by adopting Nakajima and King's algorithm (1990), we were able to retrieve δ_c and r_e from two areas further south (~35.4°N, 23.9°W), in which we believe clean maritime clouds and dirtier clouds were carefully selected. The retrieved values of δ_c and r_e for these two cloudy areas are (6, 8 μm) and (12, 6 μm), respectively. Substituting these values back into Eq. 13.4, and based on radiative transfer calculations of $\delta_c \; \partial A/\partial \delta_c = 0.22$ for both cases, together with FSSP–100 measurements of $N = 395$ cm^{-3}, we estimate the cloud susceptibility in this location to be $\sim 0.19 \times 10^{-3}$ cm^3, about a quarter of the value obtained for June12.

Table 13.1 Statistics of C–131A microphysical measurements and condensation nuclei concentrations above and below marine stratocumulus on June 12 and June 17, 1992. Includes all data times when the cloud liquid water content exceeds 0.05 g m^{-3}.

		June 12, 1992	June 17, 1992
N (cm^{-3})	mean	144	395
	median	148	393
	standard deviation	39	119
Effective Radius (μm)	mean	12.7	9.9
	median	13.3	10.1
	standard deviation	2.3	2.1
Liquid Water Content (g m^{-3})	mean	0.34	0.40
	median	0.34	0.30
	standard deviation	0.17	0.28
CN (cm^{-3})	above cloud	300	600–1200
	below cloud	200	900–1200

* CN denotes total condensation nuclei obtained from a General Electric water expansion cloud chamber at 400% supersaturation.

Note that droplet concentration is given by

$$N = \frac{3}{4\pi\rho_w}\frac{W}{r_v^3} \cong \frac{3\kappa}{4\pi\rho_w}\frac{W}{r_e^3}, \tag{13.7}$$

where κ is 0.81 ± 0.06 for maritime (0.65 ± 0.07 for continental) air masses, as suggested by Martin et al. (1994). If droplet concentration is calculated from PVM–100A measurements of effective radius and liquid water content, we estimate that $N \cong 50$ cm^{-3} on June 12 (151 cm^{-3} on June 17). The mean droplet concentration derived from FSSP–100 measurements was, instead, $N \cong 144$ cm^{-3} on June 12 (395 cm^{-3} on June 17). Therefore, cloud susceptibility deduced from PVM measurements is about 2–3 times as large as the above values, which were deduced from FSSP measurements. Furthermore, any albedo modification arising from the introduction of additional CCN into a cloud environment will be very different, as noted by a cloud's susceptibility. Whether clouds on June 17 can be said to have suffered the indirect effect is uncertain. What we can say with certainty is that the likely presence of "dirty" air has modified the cloud microphysics, as compared to the "clean" air encountered on June 12. We cannot determine unambiguously whether the cloud albedo on June 17 is larger than that of a hypothetical cloud developing in clean-air with identical forcings.

In the above analysis, we have had the luxury of using aircraft *in situ* droplet concentration measurements. Over large spatial and temporal scales, remote sensing of droplet radius using either airborne- or satellite-measured reflectances is more practical. However, inferring droplet concentration from effective radius retrievals requires an assumption about the cloud liquid water content. While large-scale averages of liquid water content are relatively constant for stratus clouds in many marine environments, there may be instances for which such an assumption can be deceiving. Such an instance can be found in the data set of June 17. An abrupt transition in cloud albedo and morphology was observed in satellite and MAS imagery on June 17. This transition boundary lay along an approximately northwest to southeast line at about 23°W, and was often thought to represent a boundary between continental air coming out of the northeast and maritime air advecting from the northwest.

Plate 13.2 shows a red (2.14 μm), green (1.62 μm), blue (0.66 μm) composite image derived from MAS data on June 17, 1992, between 1221:21 and 1227:33 UTC. In this image, the ER–2 aircraft was flying from top to bottom down the center of the image, with a heading of 304° and the MAS scanning clockwise. This image was remapped to a horizontal grid at 1 km altitude, thus providing a uniform spatial scale over the 72 × 36 km size of the image. Striking features shown in Plate 13.2 include a boundary-like broken cloud (running from upper left to lower right) that separates a clean cloud scene at the upper-right corner and a dirty cloud scene with haze layer aloft (very dense at lower-right corner). The flight track of the C–131A is indicated diagonally across the image. The C–131A was flying at an altitude of 1160–1120 m within the cloud and at an air speed of ~80 m s^{-1} (40% of the ER–2 air speed of ~200 m s^{-1}). Therefore, the C–131A was about three minutes early at the beginning of the flight line and ended about six minutes late.

Aircraft transects of measured cloud liquid water content, with a threshold value of 0.05 g m^{-3}, and effective radius are shown in Figure 13.6 for the C–131A flight. As shown in Figure 13.6a, the effective radius increases by about 6 μm as the aircraft moves westward across the microphysical transition. By itself, the increase in effective radius might suggest a transition from a continental to maritime air mass. However, the liquid water content shown in Figure 13.6b becomes out of phase with the effective radius as the aircraft crosses 23.7°W. Histograms of droplet concentration (not shown) measured west of 23.7°W are also in phase with the liquid water content. It is more likely that the western portion of the area flown by the C–131A was under the influence of a continental air mass and that the transition boundary noted in the MAS image and measured *in situ* by the C–131A was meteorological and not microphysical.

CONCLUSIONS

There has been a general concern that the potential climate forcing from the indirect effects of aerosol on clouds can be of comparable magnitude, but opposite in sign, to greenhouse-gas forcing. To estimate the magnitude of this potential albedo modification to existing clouds, we have discussed the usefulness of a figure of merit referred to as cloud susceptibility and related it to measurable cloud parameters.

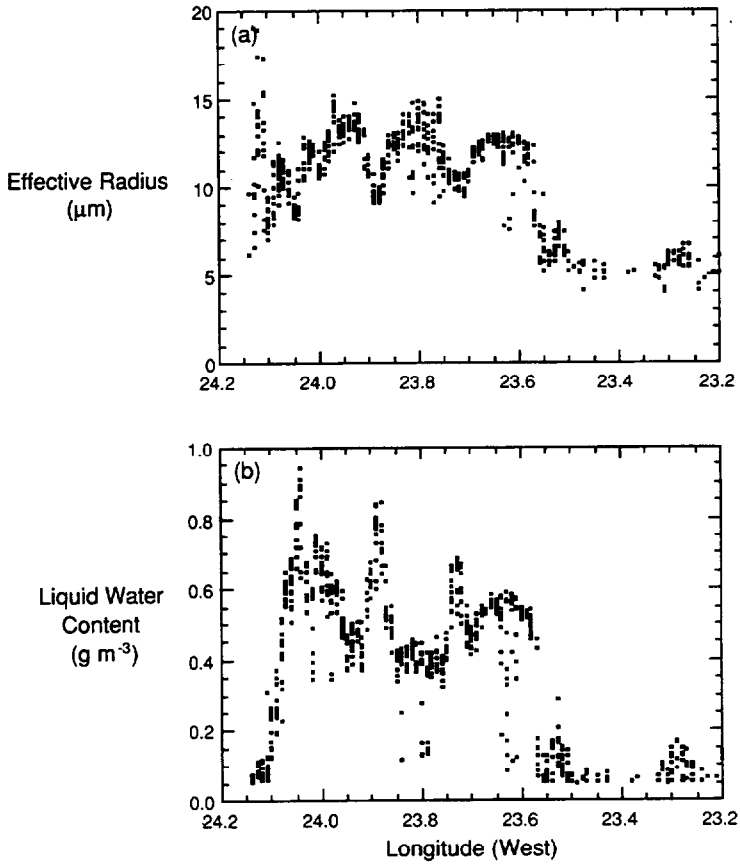

Figure 13.6 Aircraft transects in a marine stratocumulus cloud layer on June 17, 1992, showing changes in (a) effective radius and (b) liquid water content across the transition. The effective radius was derived from PVM–corrected FSSP and OAP–200X measurements, and the liquid water content from PVM–100A and OAP–200X measurements.

On examining our ability to measure the indirect effects, we find that increasing attention should be focused on new and innovative observational approaches and measurement techniques. These new approaches and instrumentation concepts, which have begun to be implemented in recent years and which have been discussed in this review, shed some light on understanding the fundamental principles of the indirect effects as well as raised a number of outstanding problems.

Ship tracks are a dramatic example of the indirect effect. We have presented a review of the first *in situ* measurements obtained of clouds modified by emissions from ships; results which agreed well with our expectations from the physical principles behind the indirect effect. Existing on a small scale, as they do, ship tracks provide a useful

laboratory for the study of cloud microphysical changes as well as tests of instrumentation and remote-sensing algorithms. The Monterey Area Ship Tracks experiment (June, 1994) will be conducted to better understand the mechanisms influencing ship track development. However, the validity of extrapolating ship track measurements to the global-scale climate problem has yet to be ascertained.

A quantitative assessment of the global indirect forcing requires knowledge of existing cloud albedo and microphysics, especially for remote maritime clouds. The only practical means of acquiring such data is through satellite remote sensing. Various remote-sensing issues still need be addressed, including cloud inhomogeneities, atmospheric corrections and extra-cloud aerosol effects, and the relationship between retrieved effective radius and droplet concentration.

ACKNOWLEDGMENT

We are grateful to Prof. P.A. Durkee of the Naval Postgraduate School for providing the AVHRR visible and shortwave infrared images of ship tracks, M. Wang of Research and Data Systems Corporation for analysis of MAS ASTEX data, J.Y. Li and G.T. Arnold of the Applied Research Corporation for aid in assembling the figures used in this manuscript, H. Gerber of Gerber Scientific for providing PVM–100 microphysical measurements, and A. Rangno and Prof. P.V. Hobbs of the Univerisity of Washington for providing FSSP–100, OAP–200X, and Johnson-Williams hot wire probe measurements. Finally, we thank Podzimek (1989) for directing our attention to Knott's (1923) book on the collected scientific papers of John Aitken, which contains the quotation cited at the beginning of this article.

REFERENCES

Ackerman, T.P., and M.B. Baker. 1977. Shortwave radiative effects of unactivated aerosol particles in clouds. *J. Appl. Meteorol.* **16:**63–69.

Aitken, J. 1880. On dust, fogs, and clouds. *Trans. Roy. Soc. Edinburgh* **30:**337–368.

Albrecht, B.A. 1989. Aerosols, cloud microphysics, and fractional cloudiness. *Science* **245:**1227–1230.

Albrecht, B.A., D.A. Randall, and S. Nicholls. 1988. Observations of marine stratocumulus clouds during FIRE. *Bull. Am. Meteorol. Soc.* **69:**618–626.

Ayers, G.P., J.P. Ivey, and R.W. Gillett. 1991. Coherence between seasonal cycles of dimethyl sulphide, methanesulphonate and sulphate in marine air. *Nature* **349:**404–406.

Baumgardner, D., W. Strapp, and J.E. Dye. 1985. Evaluation of the forward scattering spectrometer probe. II. Corrections for coincidence and dead-time losses. *J. Atmos. Oceanic Technol.* **2:**626–632.

Bigg, E.K., J.L. Gras, and C. Evans. 1984. Origin of Aitken particles in remote regions of the Southern Hemisphere. *J. Atmos. Chem.* **1:**203–214.

Bluth, R.T., and B.A. Albrecht. 1993. Atlantic stratocumulus transition experiment and marine aerosol and gas exchange June 1992 experiment summary. I. Mission summaries. Pennsylvania State Univ., Dept. of Meteorology.

Bohren, C.F. 1987. Multiple scattering of light and some of its observable consequences. *Am. J. Phys.* **55**:524–533.

Braham, R.R., Jr. 1974. Cloud physics of urban weather modification—A preliminary report. *Bull. Am. Meteorol. Soc.* **55**:100–106.

Brenguier, J.L. 1989. Coincidence and dead-time corrections for particle counters. II. High concentration measurements with an FSSP. *J. Atmos. Oceanic Technol.* **6**:585–598.

Charlson, R.J., S.E. Schwartz, J.M. Hales, R.D. Cess, J.A. Coakley, Jr., J.E. Hansen, and D.J. Hofmann. 1992. Climate forcing by anthropogenic aerosols. *Science* **255**:423–430.

Coakley, J.A., Jr., R.L. Bernstein, and P.A. Durkee. 1987. Effect of ship-track effluents on cloud reflectivity. *Science* **237**:1020–1022.

Conover, J.H. 1966. Anomalous cloud lines. *J. Atmos. Sci.* **23**:778–785.

Durkee, P.A. 1990. Global analysis of aerosol-cloud interaction: Implications for climate change processes. In: Proc. 5th Conf. on Satellite Meteorology and Oceanography, pp. 35–37. Boston: American Meteorological Society.

Gerber, H., B.G. Arends, and A. Ackerman. 1994. New microphysics sensor for aircraft use. *Atmos. Res.* **31**:235–252.

Grassl, H. 1982. The influence of aerosol particles on radiation parameters of clouds. *Időjárás, J. Hungarian Meteorol. Soc.* **86**:60–75.

Harshvardhan, and M.D. King. 1993. Comparative accuracy of diffuse radiative properties computed using selected multiple scattering approximations. *J. Atmos. Sci.* **50**:247–259.

Hegg, D.A., L.F. Radke, and P.V. Hobbs. 1991. Measurements of Aitken nuclei and cloud condensation nuclei in the marine atmosphere and their relation to the DMS–cloud–climate hypothesis. *J. Geophys. Res.* **96**:18,727–18,733.

Hobbs, P.V., L.F. Radke, and S.E. Shumway. 1970. Cloud condensation nuclei from industrial sources and their apparent influence on precipitation in Washington state. *J. Atmos. Sci.* **27**:81–89.

Hudson, J.G. 1983. Effects of CCN concentrations on stratus clouds. *J. Atmos. Sci.* **40**:480–486.

Hudson, J.G., and C.F. Rogers. 1986. Relationship between critical supersaturation and cloud droplet size: Implications for cloud mixing processes. *J. Atmos. Sci.* **43**:2341–2359.

Kaufman, Y.J., and T. Nakajima. 1993. Effect of Amazon smoke on cloud microphysics and albedo. *J. Appl. Meteorol.* **32**:729–744.

King, M.D., Y.J. Kaufman, W.P. Menzel, and D. Tanré. 1992. Remote sensing of cloud, aerosol, and water vapor properties from the Moderate Resolution Imaging Spectrometer (MODIS). *IEEE Trans. Geosci. Remote Sens.* **30**:2–27.

King, M.D., L.F. Radke, and P.V. Hobbs. 1993. Optical properties of marine stratocumulus clouds modified by ships. *J. Geophys. Res.* **98**:2729–2739.

King, M.D., M.G. Strange, P. Leone, and L.R. Blaine. 1986. Multiwavelength scanning radiometer for airborne measurements of scattered radiation within clouds. *J. Atmos. Oceanic Technol.* **3**:513–522.

Knollenberg, R.G. 1981. Techniques for probing cloud microstructure. In: Clouds: Their Formation, Optical Properties, and Effects, ed. P.V. Hobbs and A. Deepak, pp. 15–91. New York: Academic.

Knott, C.G. 1923. Collected Scientific Papers of John Aitken, LL.D., F.R.S. London: Cambridge Univ. Press.

Martin, G.M., D.W. Johnson, and A. Spice. 1994. The measurement and parameterization of effective radius of droplets in stratocumulus clouds. *J. Atmos. Sci.* **51**:1823–1842.

Nakajima, T., and M.D. King. 1990. Determination of the optical thickness and effective particle radius of clouds from reflected solar radiation measurements. I. Theory. *J. Atmos. Sci.* **47**:1878–1893.

Nakajima, T., M.D. King, J.D. Spinhirne, and L.F. Radke. 1991. Determination of the optical thickness and effective particle radius of clouds from reflected solar radiation measurements. II. Marine stratocumulus observations. *J. Atmos. Sci.* **48**:728–750.

Platnick, S., and S. Twomey. 1994. Determining the susceptibility of cloud albedo to changes in droplet concentration with the Advanced Very High Resolution Radiometer. *J. Appl. Meteorol.* **33**:334–347.

Platnick, S., and F.P.J. Valero. 1995. A validation study of a satellite cloud retrieval during ASTEX. *J. Atmos. Sci.*, in press.

Podzimek, J. 1989. John Aitken's contribution to atmospheric and aerosol sciences—One hundred years of condensation nuclei counting. *Bull. Am. Meteorol. Soc.* **70**:1538–1545.

Radke, L.F. 1989. Airborne observations of cloud microphysics modified by anthropogenic forcing. In: Proc. Symp. on the Role of Clouds in Atmospheric Chemistry and Global Climate, pp. 310–315. Boston: American Meteorological Society.

Radke, L.F., J.A. Coakley, Jr., and M.D. King. 1989. Direct and remote sensing observations of the effects of ships on clouds. *Science* **246**:1146–1149.

Radke, L.F., and P.V. Hobbs. 1976. Cloud condensation nuclei on the Atlantic seaboard of the United States. *Science* **193**:999–1002.

Rawlins, F., and J.S. Foot. 1990. Remotely sensed measurements of stratocumulus properties during FIRE using the C130 aircraft multichannel radiometer. *J. Atmos. Sci.* **47**:2488–2503.

Salomonson, V.V., W.L. Barnes, P.W. Maymon, H.E. Montgomery, and H. Ostrow. 1989. MODIS: Advanced facility instrument for studies of the Earth as a system. *IEEE Trans. Geosci. Remote Sens.* **27**:145–153.

Spinhirne, J.D., R. Boers, and W.D. Hart. 1989. Cloud top liquid water from lidar observations of marine stratocumulus. *J. Appl. Meteorol.* **28**:81–90.

Squires, P. 1966. An estimate of the anthropogenic production of cloud nuclei. *J. Rech. Atmos.* **2**:297–308.

Syrett, W.J. 1993. Low-level temperature and moisture structure from ASTEX radiosondes, 1–28 June 1992. Pennsylvania State Univ., Dept. of Meteorology.

Twomey, S. 1959. The nuclei of natural cloud formation. II. The supersaturation in natural clouds and the variation of cloud droplet concentration. *Geofisica Pura E Applicata* **43**:243–249.

Twomey, S. 1974. Pollution and the planetary albedo. *Atmos. Environ.* **8**:1251–1256.

Twomey, S. 1977. The influence of pollution on the shortwave albedo of clouds. *J. Atmos. Sci.* **34**:1149–1152.

Twomey, S. 1980. Cloud nucleation in the atmosphere and the influence of nucleus concentration levels in atmospheric physics. *J. Phys. Chem.* **84**:1459–1463.

Twomey, S. 1991. Aerosols, clouds and radiation. *Atmos. Environ.* **25A**:2435–2442.

Twomey, S., and T. Cocks. 1989. Remote sensing of cloud parameters from spectral reflectance in the near-infrared. *Beitr. Phys. Atmos.* **62**:172–179.

Twomey, S., M. Piepgrass, and T.L. Wolfe. 1984. An assessment of the impact of pollution on global cloud albedo. *Tellus* **36**:356–366.

Twomey, S., and J. Warner. 1967. Comparison of measurements of cloud droplets and cloud nuclei. *J. Atmos. Sci.* **24**:702–703.

Warner, J. and S. Twomey. 1967. The production of cloud nuclei by cane fires and the effect on cloud droplet concentration. *J. Atmos. Sci.* **24**:704–706.

Wigley, T.M.L. 1989. Possible climate change due to SO_2–derived cloud condensation nuclei. *Nature* **339**:355–357.